Chinese Journal of
POLYMER SCIENCE

RESEARCH ARTICLE

https://doi.org/10.1007/s10118-026-3695-5
Chinese J. Polym. Sci.

Molecular Segregation and Melt Memory in Dilute Polycaprolactone with Reduced Entanglements

Ce Shi[a,†], Jia-Le Zeng[b,†], Ze-Fan Wang[a,b*], and Yong-Feng Men[a,c*]

[a] *State Key Laboratory of Polymer Science and Technology, Changchun Institute of Applied Chemistry, Chinese Academy of Sciences, Changchun 130022, China*
[b] *School of Chemistry and Environmental Engineering, Shenzhen University, Shenzhen 518060, China*
[c] *School of Applied Chemistry and Engineering, University of Science and Technology of China, Hefei 230026, China*

Electronic Supplementary Information

Abstract In polymer processing, low-molecular-weight chemically identical oligomers are typically added to a polymer to improve its processability and mechanical properties by manipulating its entanglement concentration. However, the complicated semi-crystalline morphologies and melt memory effect of less entangled bimodal dispersed mixtures cannot be overlooked. In this study, we systematically examined the crystallization and self-nucleation behavior of poly(ε-caprolactone) (PCL) mixtures composed of a relatively high-molecular-weight (83 kg/mol) fraction and a low-molecular-weight PCL with a mid-chain defect (2 kg/mol). The entanglement concentrations were quantified by linear rheological measurements. Both thermal analysis and small-angle X-ray scattering (SAXS) investigations revealed that pronounced crystallization-induced phase separation (*i.e.*, molecular segregation) occurs because of the different nucleation energy barriers. In contrast to our previous investigation using a long chain fraction with a higher molecular weight (200 kg/mol) (*Macromolecules* **2024**, *57*, 1632−1641), the low-molecular-weight oligomer tends to crystallize between adjacent crystalline lamellae composed of long PCL chains due to the lack of intra-crystalline links, for example, entanglements and tie-molecules. The correlation between the melt memory effect and the entanglement concentration was evaluated using self-nucleation experiments. The 2 kg/mol PCL oligomer (with a central defect) did not exhibit melt memory. However, the introduction of high-molecular-weight components, even below the critical entanglement concentration, leads to a wider temperature range, preserving the ordered structure. Our results provide solid evidence that the melt memory effect in polar semi-crystalline polymers originates from the intramolecular interactions of adjacent chain folding rather than entanglements or chain overlaps.

Keywords Molecular segregation; Small-angle X-ray scattering (SAXS); Melt memory

Citation: Shi, C.; Zeng, J. L.; Wang, Z. F.; Men, Y. F. Molecular segregation and melt memory in dilute polycaprolactone with reduced entanglements. *Chinese J. Polym. Sci.* https://doi.org/10.1007/s10118-026-3695-5

INTRODUCTION

To improve the processability of long-chain semi-crystalline polymers in the industry, chemically identical low-molecular-weight (MW) oligomers can be added to the polymer of interest to modify its entanglement network and relaxation time.[1−4] For example, polyethylene products with bimodal molecular weight distributions are commonly used in many aspects of human life, including packaging and piping.[2,5−7] However, because of the different thermodynamic and kinetic properties of long and short chains, complex crystallization behavior often occurs at various supercoolings, resulting in different morphologies.[8,9]

In the 1970s, by investigating the isothermal crystallization behavior of polyethylene (PE) with different molecular weights and distributions, Wunderlich *et al.*[10−12] observed clear molecular fractionation during crystallization, which was strongly related to MW and crystallization temperature (T_c). To explain this phenomenon, the authors considered that every molecule must undergo a nucleation stage before assembling into crystals (*i.e.*, molecular nucleation), thereby resulting in a segregation effect. By systematically investigating the crystallization behavior of bimodal MW distribution polyethylene oxide (PEO), Cheng *et al.*[11,12] proposed that there are three distinct T_c regions in which co-crystallization or molecular segregation may occur in three distinct T_c regions. (1) *Regime I*. Crystallization temperature (T_c) is relatively high, and only the high-MW fraction can crystallize. In this case, complete separation of the high- and low-MW components was observed; (2) *Regime II*. T_c in this temperature region is moderate, and chain segregation competition occurs between the high- and low-MW fractions, resulting in partial molecular segregation; (3) *Regime III*. The driving force for crystallization in this temperature regime (large supercooling) is extremely strong, leading to the co-crystallization of high- and low-MW

* Corresponding authors, E-mail: zfwang@ciac.ac.cn (Z.F.W.)
E-mail: men@ciac.ac.cn (Y.F.M.)
† These authors contributed equally to this work.
Received March 5, 2026; Accepted April 4, 2026; Published online July 22, 2026

fractions. Subsequently, Hu *et al*.[13,14] successfully obtained similar results based on Monte Carlo simulations and established the well-known "intramolecular nucleation" model. However, the quantitative effects of entanglement and tie molecules on the crystalline morphologies have not been systematically explored.

Recently, by diluting high-MW PCL (M_w= 200 kg/mol) with oligomeric PCLs, we successfully prepared a series of uniform PCL melts with reduced entanglement concentrations.[15–17] Assuming the thickness of the amorphous layer needs to be adjusted until the maximum entanglement concentration is reached, a simple and quantitative model without adjustable parameters has been developed that can predict PCL morphology and crystallinity. At relatively small supercooling (high T_c, *regime I*), owing to strong thermodynamic segregation, low-MW components either accumulate between adjacent individual lamellae or between adjacent lamellar stacks, forming what is known as "intercrystalline segregation" or "interfibrillar segregation" structures.[18–20] In our case[17], small-angle X-ray scattering (SAXS) investigations confirmed that the gyration of the radius of the high-MW PCL fraction is large enough to cross the adjacent lamellae, forming entanglements or tie-molecules and leading to the formation of lamellar stacks. Another unresolved question arises: whether the model used to calculate the crystalline parameters of lamellar stacks remains valid when the MW of the long-chain PCL is not sufficiently high.

On the other hand, as a fundamental topic in polymer crystallization, the melt memory of semi-crystalline polymers has long been associated with crystalline morphologies, intermolecular interactions, chain topology, and entanglement networks, as it seems to be a unique property of long-chain polymeric materials.[21–25] By mixing PCL with another completely miscible dynamically asymmetric component, poly(styrene-*co*-acrylonitrile) (SAN), a matched time scale was observed between the re-entanglement kinetics and melt memory survival lifetime.[26]

Müller, Cavallo, and co-workers have systematically studied melt memory in a large series of polar homopolymers, including polyamides, polyesters, polyethers, and others.[27,28] They concluded that melt memory arises from intermolecular interactions that develop when polar chains are closely packed inside the crystals. In fact, if the interactions are not sufficiently strong, as in linear polyolefins, melt memory does not exist (as in linear high-density polyethylene, ultra-high-molecular-weight polyethylene, or isotactic polypropylene). They showed how the strength of intermolecular interactions, quantified by the solubility parameter, correlates with the width of the melt memory *Domain* (*Domain IIa*).

On the other hand, Müller, Cavallo *et al*. have studied a wide range of PEO and PCL model samples (with low dispersities) covering a molecular weight range from very short oligomers (0.4 kg/mol) to well entangled samples (with molecular weights much higher than 10 times the critical molecular weight ($M_c = 2M_e$).[29–31] Their studies have been recently complemented by careful rheological determinations of both M_e and M_c with at least 20 different molecular weight model PEO and PCL samples.[31] They observed that in both PEO and PCL samples, melt memory only develops beyond a critical chain length in oligomeric samples that crystallize in extended chain crystals. The melt memory in both PEO and PCL arises in unentangled samples with molecular weights much lower than M_e (or M_c). However, they also found that the melt memory *Domain* (*DIIa*) width significantly increases with molecular weight until it saturates at molecular weight values five times higher than M_c. These effects can be explained by considering that in samples that display melt memory, all the effects that can preserve the complexity of the melt, such as the high melt viscosity of an entangled network with concomitant long relaxation times and reduced chain diffusion, delay the formation of an isotropic melt, thereby increasing the melt memory. They proposed a chain interaction index[31] that considers all the factors that affect melt memory in polar homopolymer samples: (a) intermolecular interactions, (b) crystallinity degree (obviously, if there are more crystals, melt memory increases), and (c) molecular weight.

However, because the critical MW for entanglement and folding are very similar, it is difficult to distinguish the key contributions of these two factors. In addition, the entanglement concentration is difficult to manipulate quantitatively because it jumps to a constant value once its MW reaches its entanglement molecular weight (M_e).[32] Recently, by diluting the high-MW branched long-chain ethylene/butene-1 copolymers into low-MW PE oligomers, we observed a reduction in the melt memory temperature region width (*Domain IIa*).[33] However, the melt memory of branched polyolefin copolymers is believed to originate from the complicated segregation of crystallizable and noncrystallizable sequences during crystallization.[34–43] The presence of short PE chains dilutes both entanglement networks and overall branch fractions, leading to the simplicity of the amorphous phase structure and lower thermal stability of the self-nuclei.

In this study, we systematically investigated the complicated crystallization and melting behavior of a series of homogeneous bimodal-dispersed PCL mixtures with reduced entanglement concentrations. Quantitative control of the entanglement concentration was achieved by varying the compositions of the high- and low-MW PCL components. The peculiar molecular segregation behavior and semicrystalline morphologies were systematically investigated *via* (differential scanning calorimetry (DSC) and SAXS. In the absence of intracrystalline links (*e.g.* entanglements and tie-molecules), we expanded our understanding on the formation mechanism for the "interlamellar segregation" structures. As a model system, the correlation between the entanglement concentration and melt memory effect of PCL mixtures was also investigated. Our results are expected to clarify the physical origin of the high thermal stability of the self-nuclei in polar semicrystalline polymer systems with strong intermolecular interactions.

EXPERIMENTAL

Materials

High-molecular-weight PCL with a number-average MW of M_n= 83 kg/mol (PCL83k. M_w= 144 kg/mol, PDI=1.7, characterized by Agilent GPC) and short-chain PCL oligomers containing mid-chain ether unit defects (M_w= 2 kg/mol) were purchased from

Sigma-Aldrich Co., Ltd. Oligomer PCL2k is unentangled because its MW is lower than M_e of PCL (2443 g/mol).[16] The detailed chemical structures of the two materials are shown in Scheme 1. Mixtures made of PCL83k and PCL2k with long chain fractions (ϕ_p) from 2% to 80% were prepared by dissolving them in chloroform (at a concentration of 30 mg/mL). After stirring at room temperature for 3 h, all polymeric materials were completely dissolved. Subsequently, all samples were dried in a fume hood for approximately one week and then placed in a vacuum oven for 24 h to remove all solvents.

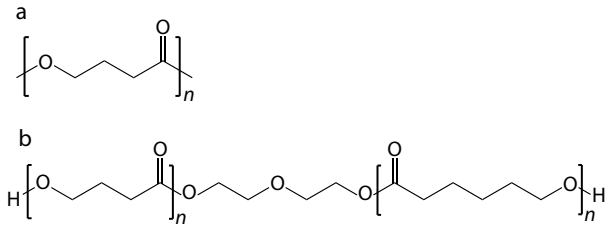

Scheme 1 Chemical structures of PCL83k (a) and PCL2k (b).

Rheological Measurements

The linear viscoelastic (SAOS) behavior of PCL83k and all mixtures was characterized using an MCR302e rheometer (Anton Paar (Austria). All measurements were performed at 90 °C with a frequency range of 628 rad/s to 0.01 rad/s. Before the experiments, all samples were hot-pressed into a 25 mm diameter disks at 90 °C for 5 min.

Differential Scanning Calorimetry

The heat flow of all PCL samples for non-isothermal, isothermal, and self-nucleation behaviors was recorded using differential scanning calorimetry (DSC) (Mettler Toledo DSC, Switzerland). The instrument was calibrated with indium prior to testing. The detailed experimental protocols are as follows.

(1) Non-isothermal crystallization. All samples were first heated to 90 °C to eliminate any possible melt memory and then cooled to 0 °C at a rate of 10 °C/min. Subsequently, the samples were heated again to the melt state.

(2) Isothermal crystallization behavior. After erasing all the thermal histories at high temperatures, all the samples were quenched at a rate of 30 °C/min to different temperatures for isothermal crystallization. After crystallization was completed, all samples were heated to melt at a rate of 10 °C/min.

(3) Self-nucleation experiments. Two types of self-nucleation thermal protocols were applied in this study, namely, standard and isothermal self-nucleation thermal protocols[25,29] as described below (shown in Fig. 1).

(a) Standard self-nucleation experiments. As illustrated in Fig. 1(a), all the samples were first heated to 90 °C to eliminate any thermal history and then cooled to 0 °C at 10 °C/min. Subsequently, the samples were heated to different self-nucleation temperatures (T_s) and held for 5 min to thermally treat them. Finally, all samples were cooled to 0 °C and heated to 90 °C again to check their crystallization and subsequent melting behavior.

(b) Isothermal self-nucleation thermal protocols. The designated PCL samples with a reduced entanglement concentration (ϕ_p=0.1) were first heated to the isotropic melt state (90 °C) to erase the thermal history. Subsequently, the samples were quenched to different T_c temperatures (35 and 30 °C) and held at these temperatures for 30 min. Subsequently, the samples were heated to different self-nucleation temperatures for 3 min to generate a homogeneous or heterogeneous melt. Finally, the PCL samples were cooled to 0 °C and heated to melt again. The detailed thermal protocol is shown in Fig. 1(b).

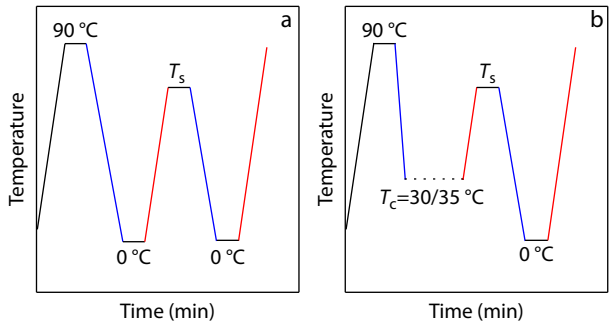

Fig. 1 Two different self-nucleation thermal protocols, namely (a) standard and (b) isothermal self-nucleation thermal protocol.

Flash Differential Scanning Calorimetry

The melting and recrystallization behavior of the PCL mixture with ϕ_p=0.2 was characterized by fast scanning calorimetry (Flash DSC1, Mettler Toledo AG, Switzerland) using an intracooler (Huber TC-100). Before the measurements, the sample was cut into small pieces and placed on the surface of the microchip. To reduce the interfacial thermal resistance between the sample and the microchip substrate, the sample was heated to 140 °C for 0.1 s and cooled to −80 °C at a rate of 1000 K/s for several cycles. The sample was first heated to 140 °C for 0.1 s to eliminate any possible thermal history, and then cooled to 20 °C at a rate of 1000 K/s and kept at that temperature for 10 min. After complete crystallization, the sample was heated to 140 °C again with different heating rates (β = 1 − 100 K/s).

Small-angle X-ray Scattering (SAXS) Experiments

Small-angle X-ray scattering experiments were performed on a laboratory beam line, Xeuss 3.0, (Xenocs, France) equipped with a Cu K_α source. Scattering profiles were recorded using an Eiger2 500k detector (Dectirs, Switzerland). Thermal treatments were controlled using a Linkam TST350 hot stage. All PCL samples were initially heated to the melt state at 90 °C, erasing any possible thermal history. Subsequently, the samples were quenched at a rate of 30 °C/min to obtain different T_c. The corresponding SAXS patterns were collected after the samples were fully crystallized. To trace the structural variation of the PCL crystals during heating, we performed *in situ* SAXS experiments. The selected PCL samples were heated to an isotropic melt at 90 °C for 5 min. Subsequently, the samples were quenched to 25 °C or 38 °C for isothermal crystallization and then heated to the melt state in steps of 2 °C. SAXS patterns were collected at each temperature.

The analysis of SAXS data for the morphologies of semicrystalline polymers is based on the interface distribution function (IDF) $K''(z)$. This method was first introduced by Ruland[44]. Thurn-Albrecht *et al.*[45–49] then further developed it and successfully established a simulation model, which not only provides information on the thickness of the crystalline

lamellae and amorphous layers, but also their distributions. Detailed descriptions can be found in Ref. [45], and here we provide a brief introduction. First, $K''(z)$ can be directly calculated from the SAXS intensity profile by

$$K''(z) = 16\pi^3 \int_0^\infty \left[\lim_{s\to\infty} I(s)\, s^4 - I(s)\, s^4 \right] \cos(2\pi s z)\, \mathrm{d}s \qquad (1)$$

where s refers to the scattering vector and $\lim_{s\to\infty} I(s)\, s^4$ is the Porod constant. On the other hand, $K''(z)$ could also be simulated by one-dimensional structure morphologies parameters, that is

$$K''(z) = \frac{O_s \Delta\rho^2}{2} \left(h_a(z) + h_c(z) - 2h_{ac}(z) + h_{aca}(z) + \ldots \right) \qquad (2)$$

$\Delta\rho$ is the electron density difference between the crystalline lamellae and amorphous phases. O_s refers to the specific inner surface area per unit volume. The thicknesses of the crystalline and layer ($d_{a,c}$) are assumed to follow a Gaussian distribution ($\sigma_{a,c}$):

$$h_{a,c}(z) = \frac{1}{\sqrt{2\pi}\sigma_{a,c}} e^{-\frac{(z-d_{a,c})^2}{2\sigma_{a,c}^2}} \qquad (3)$$

Higher-order distributions such as long-period $h_{ac}(z)$ can be calculated from the convolution of $h_a(z)$ and $h_c(z)$. Furthermore, a window function $G(s) = e^{-4\pi^2 s^2 \sigma^2}$ was applied with a constant σ value (0.8 nm) to reduce any noise.

RESULTS AND DISCUSSION

Entanglement Concentration Determined by Rheological Measurements

Fig. 2(a) shows the linear viscoelastic responses of the neat PCL83k and PCL mixture melts. All the PCL samples exhibited well-defined terminal relaxation behavior, indicating the absence of microscopic phase segregation.[50] As expected, the storage modulus (G'), loss modulus (G''), and terminal relaxation time (τ_d) decreased with an increase in the PCL2k fraction, indicating a decrease in entanglement concentration.

Unfortunately, owing to the relatively low MW of PCL83k, it is difficult to obtain the accurate plateau modulus G_0 directly from G' when G'' reaches its minimum. In our previous work[16] the plateau modulus G_0 ($f_p = 1$) of PCL was obtained by integrating the integration of G'' value using a PCL sample with a relatively high MW (200 kg/mol) and was 1.26 MPa. From this, the plateau modulus of PCL mixtures $G_0(\phi_p)$could be estimated from the G' value at the highest frequency that could be experimentally reached $G'\left(\omega_{max}, \phi_p\right)$, as follows:

$$G_0(\phi_p) = G_0(\phi_p = 1) \cdot \frac{G'\left(\omega_{max}, \phi_p\right)}{G'\left(\omega_{max}, \phi_p = 1\right)} \qquad (4)$$

On the other hand, according to polymer solution theories, $G_0(\phi_p)$ can also be obtained from the scaling law refined by Watanabe and Ruymbeke[51,52] namely $G_0(\phi_p) = G_0(\phi_p = 1) \cdot \phi_p^{\,2}$. As illustrated in Fig. 2(b), when ϕ_p was above 0.5, the calculated $G_0(\phi_p)$ roughly followed the expected scaling law (blue line). It should be noted that the PCL mixture with ϕ_p lower than 0.2 exhibit much faster relaxation owing to the dominance of the oligomer's Rouse motion and limited entanglement constraint.[52] The corresponding entanglement molecular weight of neat PCL and all mixtures $M_e(\phi_p)$ is calculated based on the rubber elasticity theory,[32, 50] as follows:

$$G_0(\phi_p) = \frac{\rho RT}{M_e(\phi_p)} \qquad (5)$$

ρ = 1.11 kg/m^3 is the density of PCL in the melt state.[16] R and T refer to the gas constant and absolute reference temperature, respectively. Fig. 2(c) illustrates the calculated $M_e(\phi_p)$ values obtained from both the measured $G_0(\phi_p)$ and

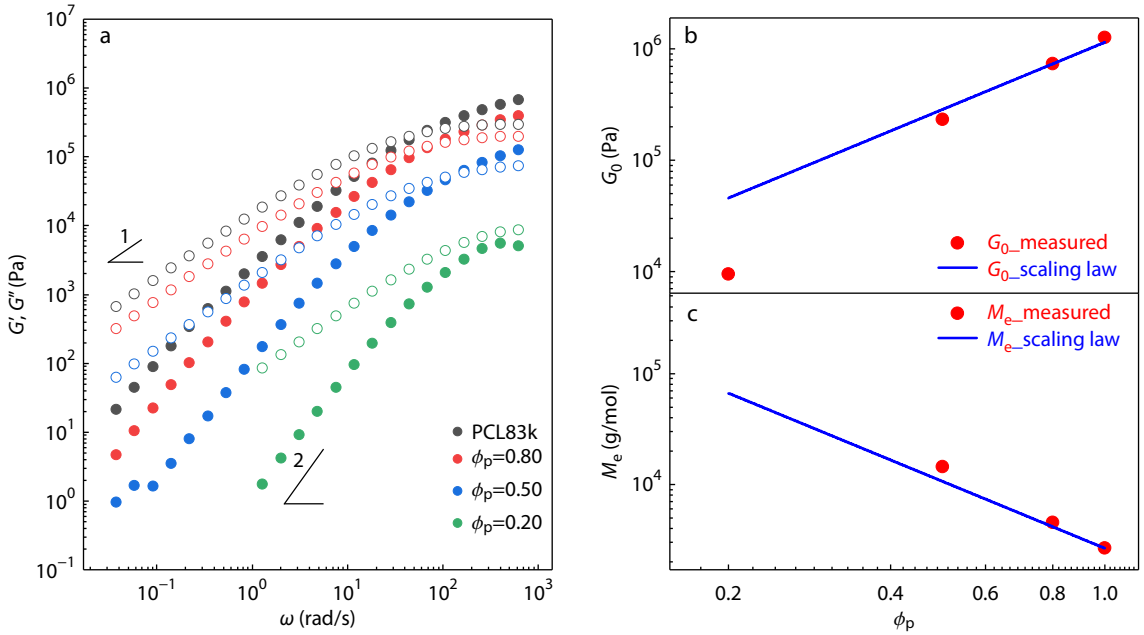

Fig. 2 (a) Linear viscoelastic behavior of PCL83k and its mixtures with PCL2k; (b) Calculated plateau modulus G_0 and (c) entanglement molecular weight M_e as a function of ϕ_p. The blue line represents the expected scaling laws for PCL mixtures.

https://doi.org/10.1007/s10118-026-3695-5

the scaling law. With the dilution process, the M_e of PCL samples gradually increases from 2.7 kg/mol to 10.6 kg/mol when ϕ_p reaches 0.5. Another important characteristic parameter, the number of entanglements per polymer chain $Z(\phi_p)$ could be estimated using M_n(PCL83k)/$M_e(f_p)$. As shown in Table S1 (in the electronic supplementary information, ESI), when ϕ_p is as low as 0.2, there are only one to two entanglements in each PCL83k chain, on average. At this point, the constraint effect of entanglement became relatively weak and negligible. Specifically, the critical entanglement fraction of PCL83k (*i.e.*, the concentration at which entanglements begin to form) can be calculated using the following equation[32]: $\phi_e = \left[M_e(\phi_p = 1)/M_n\right]^{0.76} \approx 6.8\%$. This result implies that no entanglement exists when ϕ_p is less than 0.05.

Molecular Segregation and Multiple Melting Behavior during Heating

Fig. 3 shows the DSC heating curves of the PCL samples and two of their mixtures after isothermal crystallization at different temperatures. The red, blue, and green curves represent the different melting behaviors of the PCL blends. For neat PCL83k and PCL2k (Figs. 3a and 3d), only single melting peaks ($T_{m,1}$) are observed. As expected, the value of $T_{m,1}$ increases with the increase of T_c, following the classical Hoffman-Weeks' trend.[53,54]

When 20% of low-MW PCL2k was blended with PCL83k, the PCL mixture exhibited much more complex melting behavior depending on the crystallization temperature (Fig. 3b). At a relatively low T_c=30 °C, only a single melting peak ($T_{m,2}$) appeared, representing the co-crystallization of long-chain PCL83k and low-MW PCL2k chains. When the crystallization temperature was above 35 °C, an additional low-melting peak ($T_{m,3}$) attributed to the melting of neat PCL2k lamellar crystals appeared between 40 and 45 °C, which is a clear signal of the molecular segregation phenomenon, as described by Wunderlich and Hu *et al*.[14,55,56]

A peculiar melting behavior was observed in the PCL mixtures with $\phi_p < 0.50$. As an example, Fig. 3(c) summarizes the melting behavior of the PCL sample with $\phi_p = 0.20$. It should be noted that the long PCL83k chains within the blend cannot crystallize above 45 °C. When T_c is in the range from 35 °C to 42 °C, double melting peaks ($T_{m,2}$, $T_{m,3}$) appear, which are related to the crystallization-induced phase separation behavior, as described above. On the other hand, when T_c is lower than 35 °C, in addition to the double melting peaks caused by molecular segregation, an unexpected new peak ($T_{m,1}$) appears at approximately 52 °C. There are two possibilities for generating new crystals with higher thermal stability: either they form directly at relatively low temperatures or they form through melting and recrystallization during subsequent heating.

To verify the mechanism for the formation of crystals with a higher melting peak, the melting behavior of the PCL mixture with $\phi_p = 0.20$ at various heating rates β (as shown in Fig. 4) was examined *via* a flash DSC experiment. First, the sample was isothermally crystallized at 20 °C. When β is as low as 1–2 K/s, triple melting peaks are observed, which is similar to the conventional DSC heating scan. It should be noted that the measured melting peaks in flash DSC are lower than those in

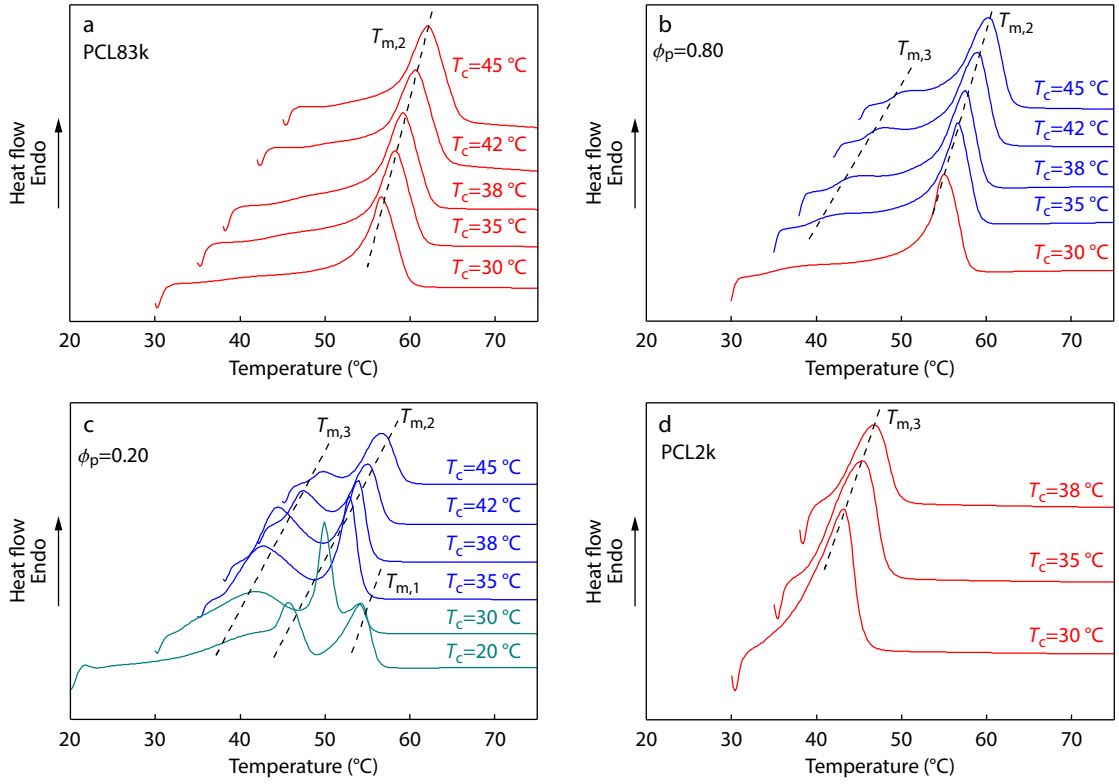

Fig. 3 DSC heating scans after isothermal crystallization at the indicated temperatures for neat PCL samples and two representative mixture compositions. (a) Neat PCL83k; (b) $\phi_p = 0.80$; (c) $\phi_p = 0.20$ and (d) neat PCL2k. The red, blue and green curves represent different melting behaviors of PCL mixtures.

https://doi.org/10.1007/s10118-026-3695-5

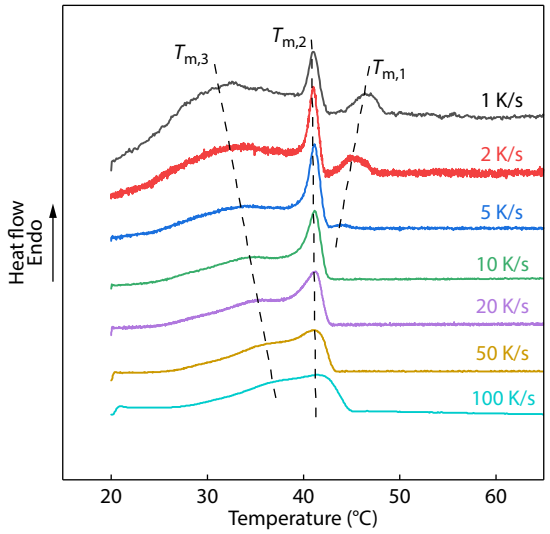

Fig. 4 Flash DSC heating run of PCL mixture with $\phi_p = 0.20$. The sample was firstly isothermally crystallized at 20 °C for 10 min and then heated to melt state with different heating rate β.

conventional DSC, owing to the different thermal lags. $T_{m,3}$ which falls in the range of 25–38 °C refers to the melting of pure low-molecular-weight fraction PCL2k crystals. The peak position shifts to a higher temperature with an increase in β owing to the superheating effect.

In the meantime, the relatively higher melting peak $T_{m,2}$ which is related to the melting of PCL co-crystals, remains almost constant at 41 °C across our heating rate range. In contrast, the occurrence of an additional melting peak $T_{m,1}$ at even higher temperatures is strongly related to β. As β increased from 1 K/s to 5 K/s, the melting enthalpy decreased dramatically, and the peak position of $T_{m,1}$ shifted to a lower temperature. In particular, peak $T_{m,1}$ completely vanishes when β reaches 10 K/s. When β is relatively low, the high MW of the PCL83k fraction has more time to re-crystallize and thicken. This clearly indicates that the crystals with such thermal stability originate from the melting and re-crystallization processes during heating rather than directly crystallizing at a relatively low temperature.[57]

Lamellar Crystalline Morphologies Characterized by SAXS

The morphology of the PCL mixtures after crystallization at different temperatures was characterized using SAXS profiles, as illustrated in Figs. 5(a)–5(c). When the crystallization temperature is lower than 30 °C (Figs. 5a and 5b), both long-chain PCL83k and low-MW PCL2k chains can crystallize because of the relatively large supercooling and the corresponding high driving force. Similar to our previous observations[16,17], the first peak, referring to the long period of crystals, shifts to the high s regime with a decrease in the long-chain PCL83k fraction. In contrast, the position of the first minimum, which reflects the form factor of the lamellar thickness, remained almost unchanged.

Figs. 5(d) and 5(e) summarize the corresponding calculated crystalline morphology parameters as functions of ϕ_p. The distribution widths of the thicknesses of the crystalline lamellae and amorphous regions are represented using error bars. The lamellar thickness d_c of PCL mixtures remains almost constant at a given T_c (approximately 5.9 and 6.2 nm at 20 and 30 °C, respectively), while the thickness of the amorphous layers d_a increases with an increase in the PCL83k fraction, ϕ_p.

In our previous work[16,17], a simple and quantitative relationship for calculating the amorphous region thickness was established based on rheological data from the scaling theory of polymer solutions. For crystal-fixed polymers such as PCL, all physical entanglements can be preserved within the inner part of the amorphous layers $d_{a,inn}$ until a maximum constant concentration $\upsilon_{e,max}$ is reached after crystallization. The boundary parts in the vicinity of crystals $d_{a,b}$ were assumed to be identical in all compositions. Therefore, the amorphous thickness $d_a(\phi_p)$ of the PCL mixtures was calculated using the following equation:

$$d_a(\phi_p) = 2d_{a,b} + \left(\frac{\upsilon_{e,max}}{\upsilon_e(\phi_p)} - 1\right)^{-1} (d_c(\phi_p) + 2d_{a,b}) \quad (6)$$

$\upsilon_e(\phi_p)$ is the entanglement strand concentration for all the mixtures with a fraction of PCL83k, f_p. According to the rubber elasticity theory and polymer solution scaling law, the entanglement concentration of PCL mixtures can be expressed

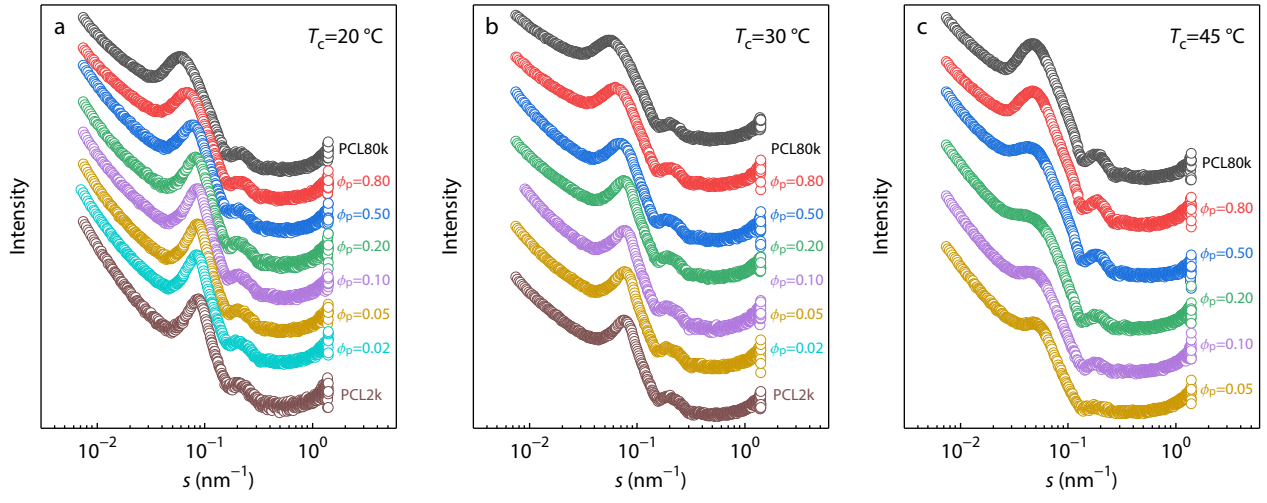

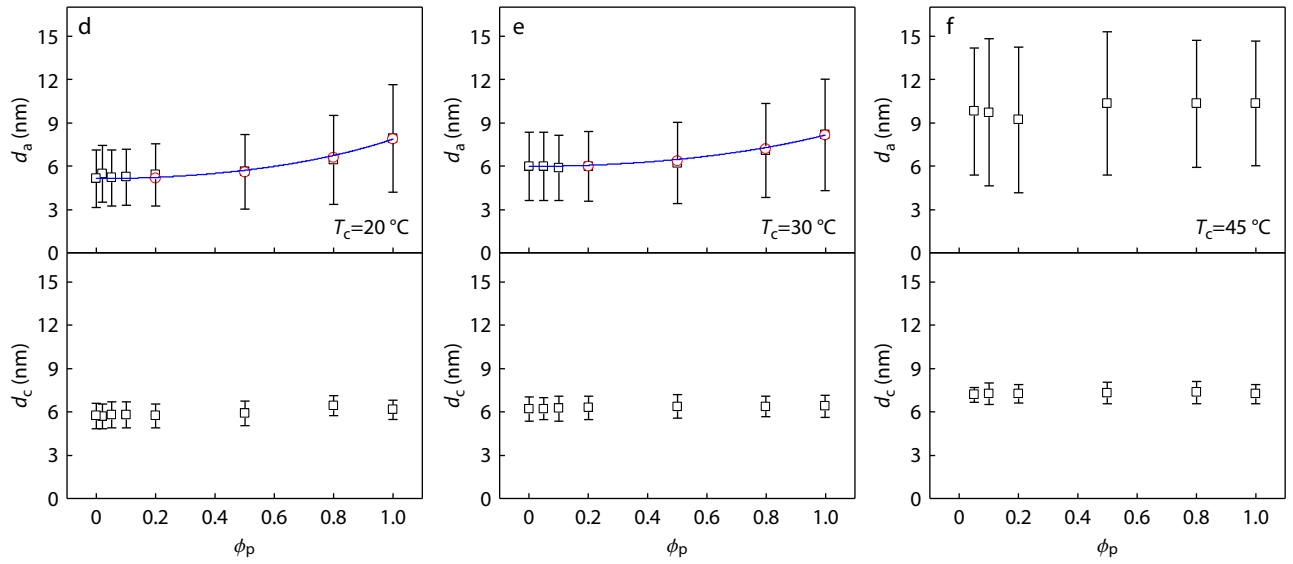

Fig. 5 SAXS profile of PCL mixtures (a–c) and the corresponding crystalline morphological parameters (d–f) analyzed based on interface distribution functions (IDF) after crystallizing at different temperatures. (a, d) T_c=20 °C; (b, e) T_c=30 °C and (c, f) T_c=45 °C. The red circle and blue line represent the calculated amorphous layer thickness d_a based on plateau modulus and scaling law, respectively.

by the plateau modulus and power law, as follows:

$$\frac{\upsilon_e(\phi_p)}{\upsilon_{e,max}} = \frac{\upsilon_e(\phi_p=1)}{\upsilon_{e,max}} \cdot \frac{\upsilon_e(\phi_p)}{\upsilon_e(\phi_p=1)} = \frac{d_{a,inn}(\phi_p=1)}{d_a(\phi_p=1)+d_c(\phi_p=1)} \cdot \frac{G_0(\phi_p)}{G_0(\phi_p=1)} = \frac{d_{a,inn}(\phi_p=1)}{d_a(\phi_p=1)+d_c(\phi_p=1)} \cdot \phi_p^2 \quad (7)$$

Below 30 °C, the calculated amorphous region thickness d_a was roughly consistent with the measured value (Figs. 5d and 5e). These results further confirm that the morphology of the crystalline lamellar stacks and their interlamellar amorphous region thickness are controlled by the entanglement networks.

The scenario is different when T_c reaches a value as high as 45 °C. At such low supercooling, neat PCL2k chains cannot nucleate and crystallize. For PCL mixtures, only a small part of the short PCL2k chain fraction can participate in the crystallization process, resulting in molecular segregation. As shown in Fig. 5(c), the peak positions of the long period remained almost at the same s position for all mixtures. Accurate IDF analysis also confirms that the amorphous layer thickness d_a maintains an almost constant value of approximately 10 nm, which is much larger than the lamellar thickness of crystals d_c (about 7.2 nm, Fig. 5f). These results reveal that PCL mixtures tend to form individual lamellae rather than a lamellar stack structure after crystallization,[19] namely so-called "interlamellar segregation" structure.

It should be noted that the results observed here are inconsistent with our previous reports using a higher-MW long-chain PCL sample (200 kg/mol).[17] We reasonably speculate that the tie molecules that are related to the coil size play a decisive role here. According to the description by Huang and Brown,[58,59] tie-molecules are more likely to form when the

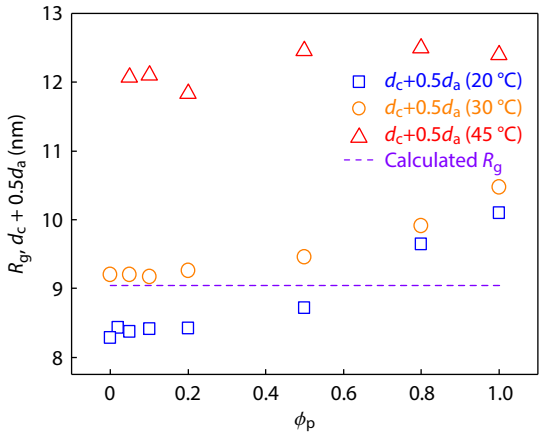

Fig. 6 Comparison of values of $d_c + 0.5d_a$ after crystallization temperatures T_cs with the radius of gyration R_g of PCL83k.

radius of gyration of the polymer chain R_g is larger than the specific space from crystalline parameters, $d_c + 0.5d_a$, that is, when the coil can penetrate adjacent lamellae. Fig. 6 compares the measured $d_c + 0.5d_a$ distances with the calculated PCL83k R_g values. The calculation of R_g for PCL83k is based on a semi-empirical equation from the literature,[60] $R_g = 0.032 \cdot \sqrt{M_n}\left(\text{nm}\sqrt{\text{mol/g}}\right) \approx 9.21$ nm. When the crystallization temperature is lower than 30 °C, the distance $d_c + 0.5d_a$ increases slowly with an increase in the PCL83k fraction ϕ_p and is in the range from 8.0 nm to 10.5 nm, which is equivalent to R_g of PCL83k. Considering the relatively wider distributions of both these parameters, it is reasonable to infer that the tie molecules are largely retained within the lamellae stacks, functioning as intra-crystalline linkers connecting the adjacent crystals. When the crystallization temperature was as high as 45 °C, the resultant value of $d_c + 0.5d_a$ was much larger than that R_g of PCL83k. In this situation, intra-crystalline links such as entanglement and tie-molecules

https://doi.org/10.1007/s10118-026-3695-5

between adjacent crystalline lamellae no longer exist, resulting in a large and nearly constant distance of long-period d_{ac}.

Structure Evolution during Heating: *In situ* SAXS Experiments

To investigate the spatial distribution of different PCL crystals in PCL mixtures, *in situ* SAXS experiments were performed on three selected PCL samples during heating: neat PCL83k, mixture with ϕ_p=0.10, and neat PCL2k. As shown in Figs. 7(a)–7(c) and Figs. S2(a)–S2(c) (in ESI), all the samples were initially crystallized at 25 and 38 °C, respectively. The corresponding crystalline morphological parameters as a function of temperature are shown in the upper panels of Figs. 7(d)–7(f) and Figs. S2(d)–S2(f) (in ESI). Additionally, the Porod constant P (lower panels of Figs. 7d–7f and Figs. S2d–S2f in ESI), which indicates changes in crystallinity, was also compared.[45,46,48]

For PCL83k, as previous reports by Thurn-Albrecht,[46,61] PCL crystals undergo successive melting and recrystallization. As depicted in the upper panel of Fig. 7(d), with an increase in temperature, the lamellar thickness of the PCL crystals d_c increases from approximately 6.3 nm to 7.3 nm. In the meantime, the size of the amorphous region increases continuously from 7.9 nm to 19.7 nm due to the random melting of the crystalline lamellae. Consequently, the value of P increases slightly from 25 °C to 35 °C, followed by a rapid decrease before complete melting. In contrast, owing to the constraint of the chain length, the temperature range for melting and recrystallization of low-molecular-weight PCL2k is relatively short, leading to a final melting temperature of approximately 45 °C (Figs. 7c and 7f). As the temperature increased, d_c and d_a increased to 7.2 and 16.4 nm, respectively.

Compared with monodispersed PCL samples, the variation in crystalline morphological parameters for the PCL mixture with ϕ_p=0.1 is more complicated. According in Fig. S1 (in ESI) three melting peaks appear in the DSC heating scan after the sample is isothermally crystallized at T_c = 25 °C. As depicted in Fig. 7(e), before reaching 41 °C, both d_a and d_c increased slowly, with a slight increase in P value. This observation is similar to that observed for neat PCL83k and PCL2k lamellar crystals owing to melting and recrystallization. Subsequently, at approximately 45 °C, the thickness of the amorphous re-

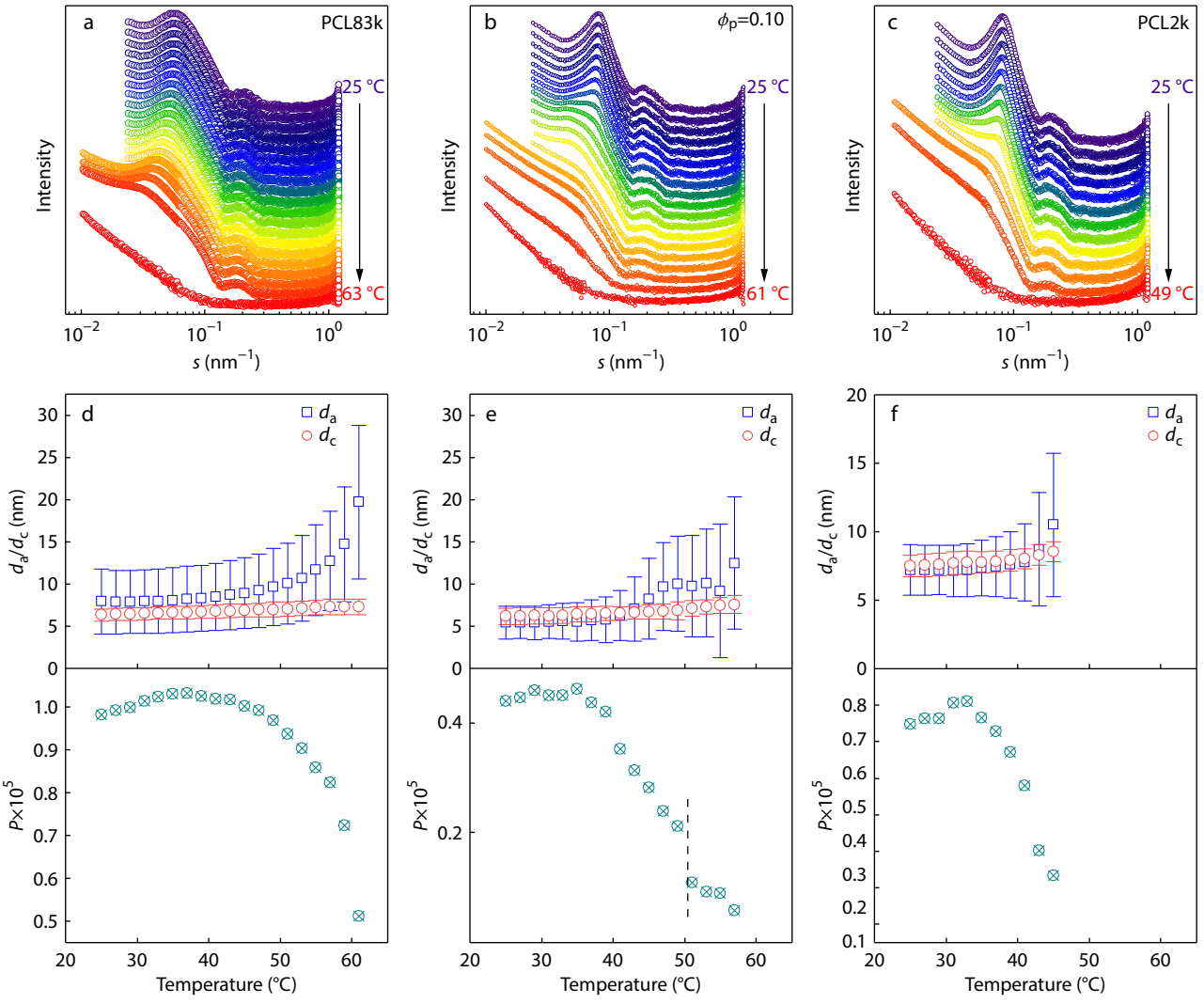

Fig. 7 SAXS intensity profiles (a–c) and the corresponding analyzed crystalline parameters, Porod constant (d–f) for PCL83k, PCL mixture with ϕ_p=0.10, and PCL2k during the heating process. The error bars represent the distribution of d_c and d_a. All samples were initially crystallized at 25 °C.

https://doi.org/10.1007/s10118-026-3695-5

gion d_a in Fig. 7(e) jumps from 6.2 nm to 7.7 nm because of the melting of the low-molecular-weight PCL2k crystals. The increase in d_a provides solid evidence that the lamellar fraction with only PCL2k chains is located between PCL crystalline lamellae containing long PCL83k chains. Above 47 °C, the d_a value reached a second plateau at approximately 10 nm before the final melting. At approximately 50 °C, the Porod constant P (lower panel of Fig. 7e) suddenly jumps from 0.212×10^{-5} to 0.11×10^{-5} at around 50 °C (indicated by the dashed line), and then plateaued. This transition temperature is believed to be related to the melting and recrystallization of long-hain crystals.

We also examined the scenario in which T_c was as high as 38 °C as illustrated in Fig. S2 (in ESI). The crystalline morphological parameters, d_a and d_c exhibited very similar variation trends across all three samples, as they crystallized at 25 °C. In particular, for PCL mixture with low entanglement concentration (ϕ_p=0.10), d_a jumps from 6.2 nm to 10.8 nm at around 45 °C, giving further evidence that low molecular weight of PCL2k crystallizes within the adjacent long chain crystalline lamellae. In addition, at higher temperatures, the variation in d_a and d_c showed almost no difference compared to that at 25 °C.

From the SAXS analysis, simplified sketches of the structural evolution of the low-entangled PCL mixture after crystallization at different temperatures are shown in Fig. 8. When T_c is as high as 45 °C (Fig. 8a), owing to the lack of tie molecules and entanglements, the high molecular weight of the PCL200k fraction and the small amount of short PCL2k chains could co-crystallize into the same individual lamellae, while the rest of the molten short chains remain in between, forming a so-called "interlamellar segregation" structure. However, at a relatively low T_c (below 38 °C, Fig. 8b), both PCL200k and PCL2k chains can be crystallized simultaneously. Because of the constraint effect of the mid-chain defect and the resultant short crystallizable chain segment, the low-molecular-weight PCL2k could only be crystallized in the extended-chain state. In this case, the low molecular weight fractions have difficulty overcoming the relatively high energy barrier by arranging into crystals composed of high molecular weight PCL200k chains.[14] Therefore, they are inclined to form individual lamellae that are sandwiched between long-chain crystalline lamellae. During the subsequent heating run, the PCL2k crystals with a relatively low thermal stability melted first, resulting in a large distance from the amorphous phase.

Standard Self-nucleation Behaviors of PCL with Reduced Entanglement Concentration

To examine the effect of entanglement on the melt memory effect, standard DSC self-nucleation experiments were performed on PCL samples with different compositions. The detailed thermal protocols are discussed in the experimental section.

The self-nucleation method in polymer science was originally developed by Blundell, Keller, and Kovacs[62,63] in their pioneering work on self-seed single crystals grown from solution with the aim of controlling their size. In a later seminal work from the Strasbourg polymer group led by Prof. Bernard Lotz (Fillon *et al.*[64], the authors designed a comprehensive thermal protocol to study self-nucleation by differential scanning calorimetry (DSC). The self-nucleation thermal protocol applied in conventional DSC is the most sensitive tool for studying self-nucleation in polymers.[38]

Fillon *et al.*[64] defined three self-nucleation *Domains*.

(1) *Domain I (melting Domain)*. In this temperature *Domain*, the self-nucleation temperature T_s was sufficiently high to erase the thermal history. Thus, an isotropic melt can be ob-

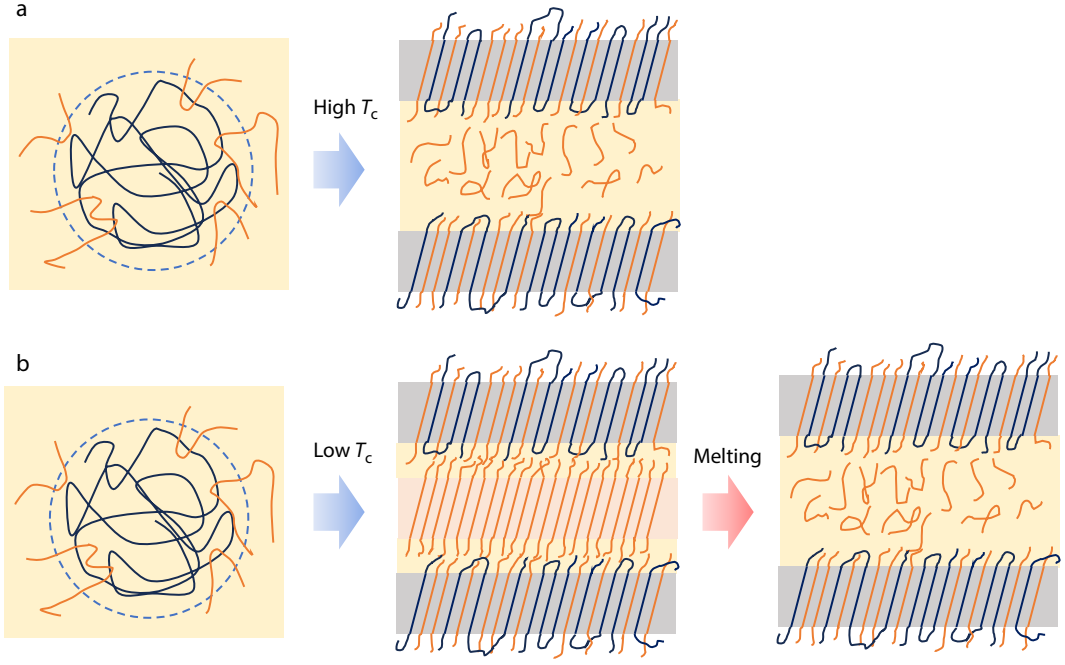

Fig. 8 Simplified sketches illustrating the crystalline structure variation of PCL mixture with low entanglement concentration (*e.g.* ϕ_p=0.10) during crystallization and subsequent heating process: (a) and (b) represent different scenarios at relatively high and low T_c, respectively.

https://doi.org/10.1007/s10118-026-3695-5

tained by melting all possible self-nuclei.

(2) *Domain II (self-nucleation Domain)*. The self-nucleation temperature T_s in this *Domain* was not sufficiently high to melt all self-nuclei. In the original work of Fillon *et al*.[64] who employed isotactic polypropylene, the authors proposed that small crystal remnants or self-seeds were the origin of the self-nucleation effect (and increase in nucleation density) detected in *Domain II*. The self-seeds generated in *Domain II* are incapable of annealing at T_s.

(3) *Domain III (self-nucleation and annealing Domain)*. The T_s temperature in this *Domain* is very low, and the crystals can only be partially melted. The residual crystals were annealed while being kept at the selected T_s temperatures.

Müller *et al*.[25,38] realized that *Domain II* should be divided into two sub-*Domains* (*Domain IIa* and *Domain IIb*) because of the different physical origins of melt memory and self-seeding: (a) *Domain IIa,* or the melt memory *Domain,* is located in the upper temperature range of *Domain II*, where all crystals have been melted in the absence of a calorimetric signal in the DSC (also corroborated by WAXS). Self-nucleation is thus caused in *DIIa* by the melt-memory-ordered regions within the self-nucleated melt. (b) *Domain IIb*, or the self-seeding *Domain,* is located in the lower temperature range of *Domain II*, in a temperature region where the material does not melt completely. The remaining crystal fragments were epitaxially perfect self-seeds that were capable of self-nucleating the material. It is clear that the self-nucleation *Domain*, or *Domain II* contains both a melt-memory temperature range (*DIIa*) and a self-seeding temperature range (*DIIb*).

The self-nucleation behaviors of all the PCL samples with different compositions are summarized in Figs. S3–S10 (in ESI). DSC curves at different temperature *Domains* are differentiated by different colors (red for *DI*, blue *DII* and green for *DIII*). According to the experimental results, the correlation between crystallization temperature T_c and self-nucleation temperature T_s for PCL samples with different compositions is illustrated in Fig. 9 with a comparison of standard heating curves. The critical self-nucleation temperatures dividing *Domain I/Domain IIa, Domain IIa/Domain IIb* and *Domain IIb/Domain III* are labeled as $T_{I,IIa}$, $T_{IIa,IIb}$ and $T_{IIb,III}$, respectively, and are marked by dashed lines.

Müller *et al*. have shown that PCL homopolymers without main-chain defects, with low polydispersity (M_w/M_n=1.1) and M_n values equal to 2000 g/mol, exhibit melt memory even with different chain ends.[29,31,65] In fact, in a recent study,[31] Müller *et al*. determined using PCL model samples that the critical molecular weights for the development of melt memory in PCL are M_n=0.96 kg/mol and M_w=1.26 kg/mol. The PCL2k oligomer employed in this work was a sample with a central ethylene glycol moiety (see Scheme 1b), which can be considered a defect at the chain center. The sample had an M_w of 2 kg/mol, but did not exhibit any melt memory (see Fig. S10 in ESI and Fig. 9h). The central defect was likely responsible for the PCL2k sample's lack of melt memory. On the other hand, the high-molecular-weight PCL homopolymer PCL83k exhibited melt memory, as expected, displaying a relatively moderate *DIIa* width of 5 °C (Fig. S3 in ESI and Fig. 9a).

Fig. 9 shows how adding a small amount of PCL2k oligomer to PCL83K increased the melt memory even below the entanglement threshold. According to the above discussions, the critical entanglement fraction of PCL83k, ϕ_e of our PCL mixtures was approximately 7.6%, above the polymer fraction of PCL mixtures with ϕ_p=5% and 2%.

Fig. 10 summarizes the correlation between the SN temperature domains as a function of ϕ_p based on the SN results illustrated in Fig. 9. It is clear that for pure PCL83k and PCL mixtures, the values of $T_{I,IIa}$ fluctuated in the range of 63–67 °C, indicating nearly identical thermal stability of the self-nuclei in all PCL mixtures. The critical temperatures $T_{IIa,IIb}$ increased from 54.5 °C to 64.2 °C as f_p increased from 2% to 100%. As a result, the width of *Domain IIa* ΔT_{IIa} decreased with increasing PCL83k fraction. The value of $T_{IIb,III}$ which is associated with the melting temperature of PCL mixtures, increased slowly from 52 °C to 55 °C. Therefore, the width of *Domain IIb* ΔT_{IIb} shows an opposite trend, increasing with an increase in the high molecular weight fraction PCL83k ϕ_p. In summary, all PCL mixtures and pure PCL83k exhibited almost identical wide *Domain II* temperature ranges, $\Delta T_{II} = \Delta T_{IIa} + \Delta T_{IIb}$, which are approximately 10–15 °C. In contrast, the defect-free neat PCL2k sample only exhibits a rather narrow *Domain IIb* (about 1 °C) without any melt memory. Note that the proportion of PCL83k in the most diluted PCL mixture (2%) is even lower than the overlap concentration $\phi^* \approx N_k^{-0.5} \approx 3.6\%$. Our results provide clear evidence that the presence of long-chain PCL83k is responsible for the high stability of self-nuclei and the corresponding wide melt memory temperature domain, rather than entanglements and chain overlap. In the literature,[29,30,66] the increment of melt memory strength (*i.e.*, the width of *Domain IIa*) is observed to be promoted when the MW reaches a critical value, which is close to the entanglement MW (M_e) or critical MW for a once-fold. However, it is difficult to determine the key factor because the two critical MW values are almost identical, and the critical MW for chain folding is difficult to precisely measure. Our findings irrefutably reveal that the state of entanglement is not responsible for generating melt memory. These results are also consistent with the recent observation by Müller *et al*.[31] that some oligomers with molecular weights even below M_e exhibit a certain temperature range of *Domain II,* which could be enhanced by chain entanglements.

Another important feature that should not be neglected is that the observations made in this study using dilute PCL mixtures are inconsistent with our previous publication[33] focusing on ethylene/butene-1 random copolymers with reduced entanglement concentration, that is, the melt memory strength decreases with decreasing long-chain fraction. It is believed that nano-sized segregation between crystallizable and non-crystallizable sequences during crystallization determines the occurrence of melt memory in non-polar polyolefin copolymers. The introduction of a low MW fraction not only dilutes the entanglement concentration but also dilutes the overall non-crystallizable sequence, resulting in reduced complexity of the polymer melt and lower thermal stability of the self-nuclei.

However, for PCL mixtures without phase separation, their relatively strong melt memory is generally considered to originate from the strong intermolecular/intramolecular interactions induced by the polarity of the monomers rather than entanglements.[28,67,68] It is reasonable hypothesize that rela-

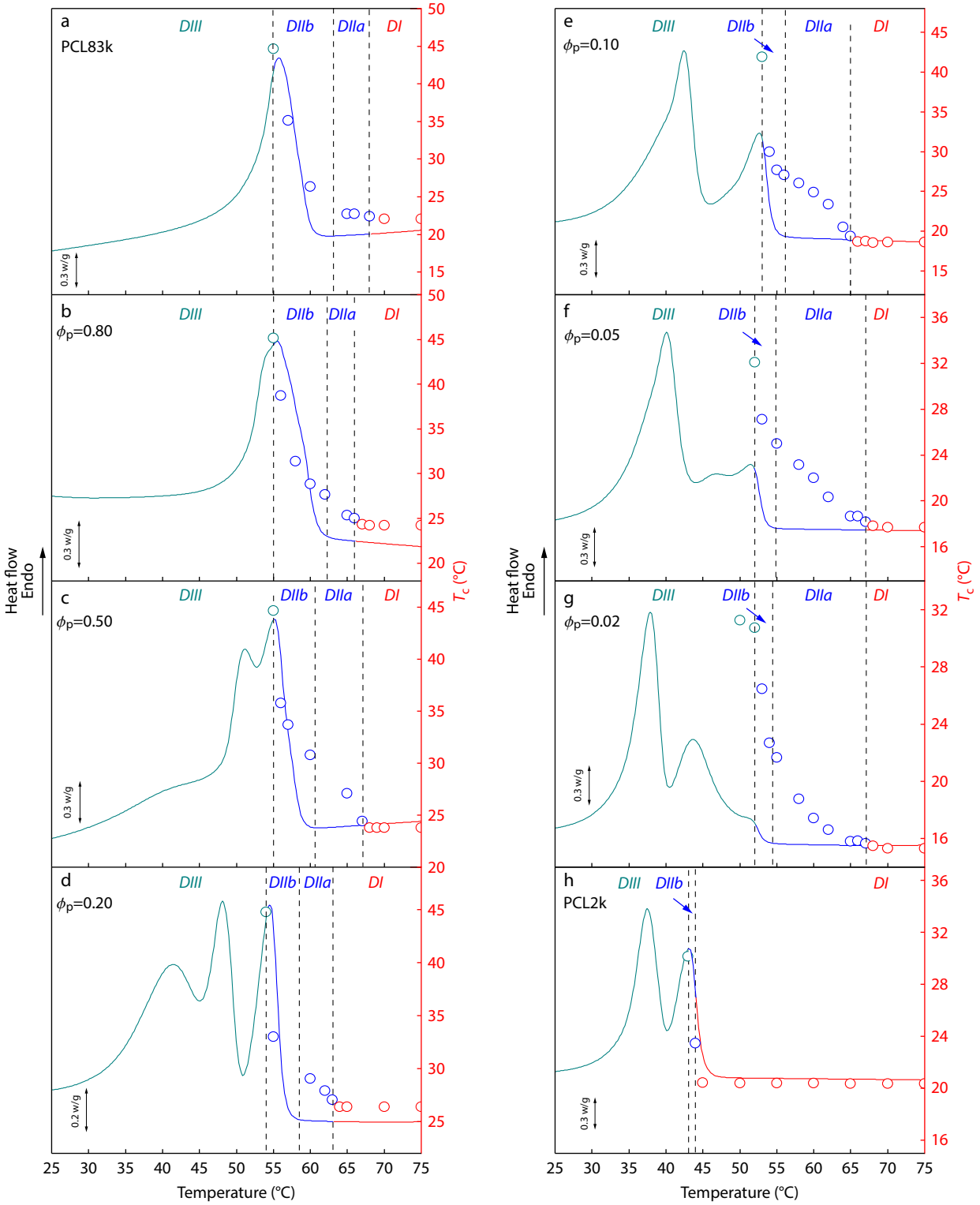

Fig. 9 Representation of three SN domains superposed on standard DSC heating scans for all PCL samples. Closed symbols refer to crystallization temperature T_c (right-handed *y*-axis) as a function of T_s value. (a) PCL83k, (b) ϕ_p=0.80, (c) ϕ_p=0.50, (d) ϕ_p=0.20, (e) ϕ_p=0.10, (f) ϕ_p=0.05, (g) ϕ_p=0.02, (h) PCL2k.

tively large number of adjacent folding number in polymer mixtures with low ϕ_p providing larger opportunities preserving the ordered sequences after melting, resulting in strong melt memory effect. Our results are also consistent with the basic knowledge that polymer nucleation occurs at the length scale, which corresponds to a Rouse motion smaller than the entanglements.[69] Existing short-range-ordered structures with high thermal stability can effectively promote

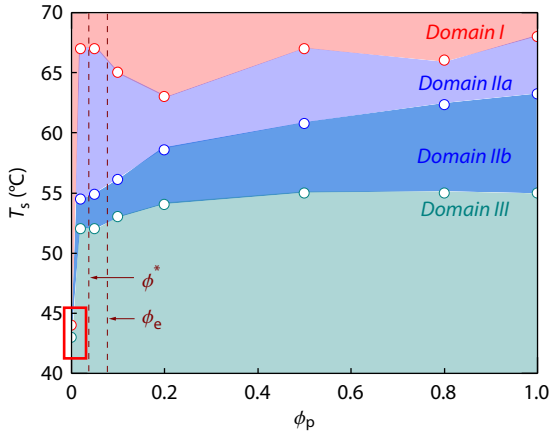

Fig. 10 Summary of the SN Domains present PCL mixtures as a function of ϕ_p. The different temperature domains are separated by the transition temperatures $T_{I,IIa}$, $T_{IIa,IIb}$ *and* $T_{IIb,III}$ by red, blue and green open symbols, respectively.

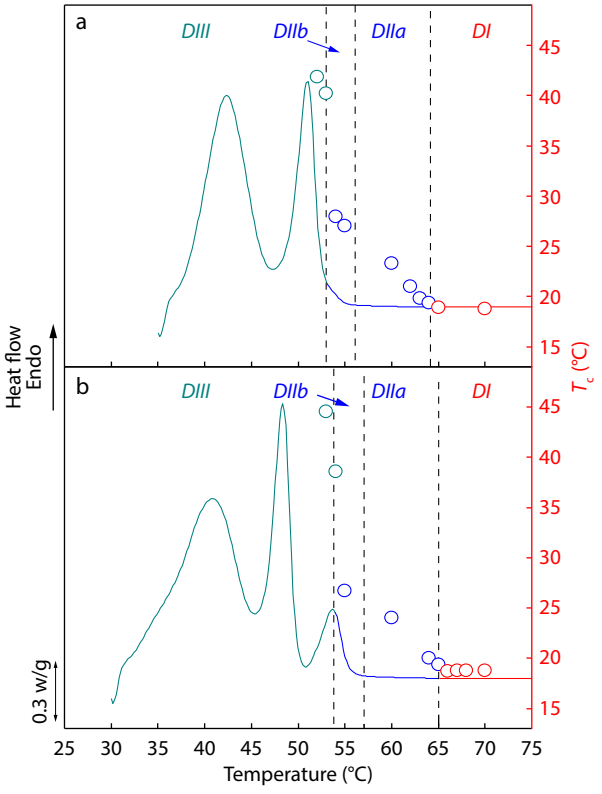

Fig. 11 Representation of three SN domains superposed on standard DSC heating scans for highly dilute PCL mixture with ϕ_p=0.10. Before the self-nucleation experiments, the sample was first crystallized at 35 (a) and 30 °C (b), respectively. Closed symbols refer to crystallization temperature T_c (right-handed *y*-axis) as a function of T_s value.

the nucleation and crystallization of long-chain polymers. Furthermore, these findings further explain that melt memory is not observed in non-polar homopolymers, such as ultra-high molecular weight polyethylene with different entanglement states, because of the weak van der Waals interactions between adjacent folds.[70–72]

Isothermal Self-nucleation Results of Highly Dilute PCL Mixtures: the Effect of Melting and Recrystallization

Another open question remaining no answer is whether the apparent melt and recrystallization behavior can significantly affect the melt memory of dilute PCL mixtures. Therefore, modified isothermal SN experiments were performed on a specific dilute PCL mixture with ϕ_p=0.10. The sample was first isothermally crystallized at 35 and 30 °C, respectively, followed by standard self-nucleation thermal protocols. As mentioned above (Fig. S1 in ESI), pronounced melt and recrystallization behaviors occurs at T_c =30 °C. Detailed SN results are shown in Figs. S11 and S12 (in ESI). The sample exhibited a relatively strong melt memory effect with a wide *Domain II* region after crystallization at both temperatures.

The corresponding crystallization temperature T_c as a function of T_s is summarized in Fig. 11, with a comparison of the standard DSC heating curves. Clearly, after isothermal crystallization at different temperatures, the dilute PCL sample exhibits almost identical self-nucleation and strong melt memory behaviors, as well as the critical self-nucleation temperatures $T_{I,IIa}$ ≈53.0 °C, $T_{IIa,IIb}$ ≈56.0 °C and $T_{IIb,III}$ ≈64.2 °C. Our results show that relatively slow melting and recrystallization have nearly no pronounced influence on the thermal stability of self-nuclei, and more energy is needed to destroy the strong intramolecular interactions caused by adjacent chain folding in polar semicrystalline polymers.

CONCLUSIONS

In this work, we present detailed investigations of the crystallization and melting behavior of bimodal PCL mixtures with different compositions. Rheological experiments confirmed that the entanglement concentration of the PCL mixtures decreased with an increase in the unentangled oligomer PCL2k fraction. The nanoscale crystallization morphologies were characterized *via* SAXS and carefully analyzed using interface distribution functions (IDF). At relatively low T_c (20 and 30 °C), where both PCL83k and PCL2k co-crystallize, PCL mixtures can form lamellar stack structures. Quantitatively, the thickness of the amorphous layer is controlled by the entanglement concentration, as described in our previous work.[16,17] On the other hand, at a relatively low supercooling temperature (T_c=45 °C), the PCL mixture tends to crystallize into individual lamellae with large amorphous regions. In this case, the chain coil size of PCL83k is relatively small and cannot penetrate two adjacent crystalline lamellae, resulting in the absence of intra-crystalline kinks, that is, entanglements and tie molecules.

Detailed self-nucleation experiments revealed that the presence of even a tiny fraction of long chains (even below ϕ_e and ϕ^*) leads to the formation of stable self-nuclei after melting, causing strong melt memories. These results provide solid evidence that intramolecular interactions of adjacent chain folds generate the melt memory effect in polar semicrystalline polymers, rather than entanglements or chain overlap.

Conflict of Interests

The authors declare no interest conflict.

https://doi.org/10.1007/s10118-026-3695-5

Electronic Supplementary Information

Melt structural property parameters calculated from rheological measurements, DSC heating curves of dilute PCL after crystallization at different temperatures, SAXS profiles during *in situ* heating and detailed self-nucleation DSC curves are provided in the electronic supplementary information (ESI). ESI is available free of charge in an online version of this article at https://doi.org/10.1007/s10118-026-3695-5.

Data Availability Statement

The related data of this paper is data that should not be shared, and can be obtained from the corresponding author for reasonable reasons.

ACKNOWLEDGMENTS

This work was financially supported by the National Natural Science Foundation of China (No. 22303052) and the Shenzhen Natural Science Foundation Project (No. JCYJ20250604181237049). We thank Prof. Alejandro J. Müller for the fruitful discussion.

REFERENCES

1 Wu, W. L.; Jong, L.; Hanyu, A.; Coyne, L. D.; Stein, R. S. Molecular structure of bimodal polymer networks. *Macromolecules* **1990**, *23*, 351–353.
2 Liu, H.-T.; Davey, C. R.; Shirodkar, P. P. Bimodal polyethylene products from UNIPOLTM single gas phase reactor using engineered catalysts. *Macromol. Symp.* **2003**, *195*, 309–316.
3 Balzano, L.; Rastogi, S.; Peters, G. Self-nucleation of polymers with flow: the case of bimodal polyethylene. *Macromolecules* **2011**, *44*, 2926–2933.
4 Men, Y. F.; Rieger, J.; Strobl, G. Role of the entangled amorphous network in tensile deformation of semicrystalline polymers. *Phys. Rev. Lett.* **2003**, *91*, 4.
5 Li, W.; Guan, C.; Xu, J.; Chen, Z.-r.; Jiang, B.; Wang, J.; Yang, Y. Bimodal/broad polyethylene prepared in a disentangled State. *Ind. Eng. Chem. Res.* **2014**, *53*, 1088–1096.
6 Sattari, M.; Inn, Y.; Wood-Adams, P. M. Wall slip of bimodal polyethylene. *Macromolecules* **2022**, *55*, 4568–4577.
7 Zou, C.; Wang, Q.; Si, G.; Chen, C. A co-anchoring strategy for the synthesis of polar bimodal polyethylene. *Nat. Comm.* **2023**, *14*, 1442.
8 Ma, Y.; Niu, D.; Liu, J.; Liu, B.; Xu, P.; Jiao, X.; Yang, W.; Liu, T.; Ma, P. Branching-density dependent chain relaxation and orientated crystallization behavior of the stretched polylactic acid melt. *Macromolecules* **2025**, *58*, 5674–5687.
9 Wang, J.; Niu, D.; Yu, T.; Xu, P.; Yang, W.; Ma, P. Highly oriented

Graphical Abstract

Molecular Segregation and Melt Memory in Dilute Polycaprolactone with Reduced Entanglements

Ce Shi, Jia-Le Zeng, Ze-Fan Wang, and Yong-Feng Men

Changchun Institute of Applied Chemistry, Chinese Academy of Sciences; Shenzhen University; University of Science and Technology of China

This study clarifies that in bimodal polymer mixtures with low entanglement concentrations, the crystallization morphology is strongly related to the molecular weight of the long chains. The lamellar stack structure is determined by the fraction of tie chains. The melt-memory effect has been proven to be related to intrachain interactions rather than entanglements.

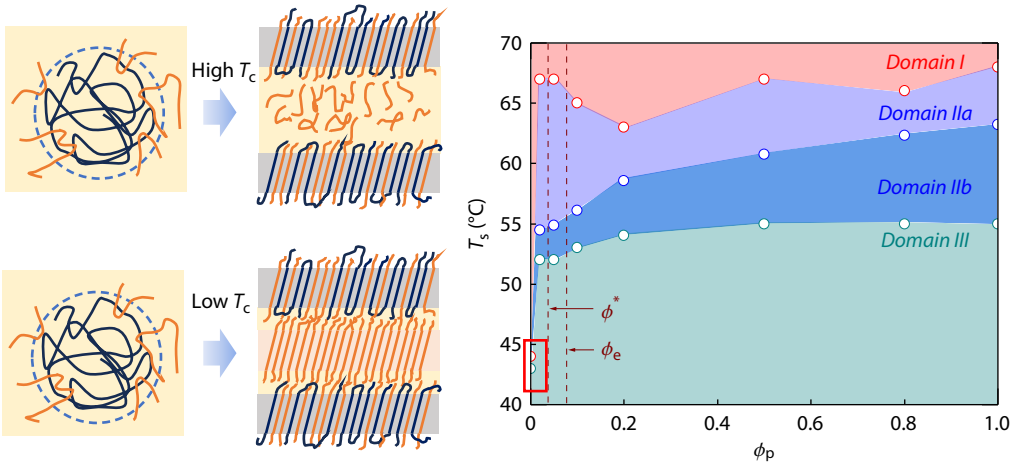

Chinese J. Polym. Sci., 2026 *https://doi.org/10.1007/s10118-026-3695-5*

polymorphism in polyglycolic acid *via* coupling of chain Entanglement and extensional strain. *Macromolecules* **2026**, *59*, 3431−3443.
10 Glaser, R. H.; Mandelkern, L. On the fractionation of homopolymers during crystallization from the pure melt. *J. Polym. Sci. B: Polym. Phys.* **1988**, *26*, 221−234.
11 Cheng, S. Z. D.; Wunderlich, B. Molecular segregation and nucleation of poly(ethylene oxide) crystallized from the melt. 1. calorimetric study. *J. Polym. Sci. B: Polym. Phys.* **1986**, *24*, 577−594.
12 Cheng, S. Z. D.; Wunderlich, B. Molecular segregation and nucleation of poly(ethylene oxide) crystallized from the melt. 2. kinetic-study. *J. Polym. Sci. B: Polym. Phys.* **1986**, *24*, 595−617.
13 Hu, W.; Frenkel, D.; Mathot, V. B. F. Intramolecular Nucleation model for polymer crystallization. *Macromolecules* **2003**, *36*, 8178−8183.
14 Hu, W. B. Molecular segregation in polymer melt crystallization: Simulation evidence and unified-scheme interpretation. *Macromolecules* **2005**, *38*, 8712−8718.
15 Saalwächter, K.; Thurn-Albrecht, T.; Paul, W. Recent progress in understanding polymer crystallization. *Macromol. Chem. Phys.* **2023**, *224*, 2200424.
16 Wang, Z.; Schaller, M.; Petzold, A.; Saalwächter, K.; Thurn-Albrecht, T. How entanglements determine the morphology of semicrystalline polymers. *Proc. Natl. Acad. Sci.* **2023**, *120*, e2217363120.
17 Wang, Z.; Schaller, M.; Petzold, A.; Saalwächter, K.; Thurn-Albrecht, T. Origin of lamellar stack structures in dilute semicrystalline polymers: role of entanglements and tie-molecules. *Macromolecules* **2024**, *57*, 1632−1641.
18 Bristow, J. F.; Kalika, D. S. Investigation of semicrystalline morphology in poly(ether ether ketone)/poly(ether imide) blends by dielectric relaxation spectroscopy. *Polymer* **1997**, *38*, 287−295.
19 Pan, P.; Zhao, L.; Yang, J.; Inoue, Y. Fractional Crystallization and phase segregation in binary miscible poly(butylene succinate)/poly(ethylene oxide) crystalline blends: effect of crystallization temperature. *Macromol. Mater. Eng.* **2013**, *298*, 201−209.
20 Wang, J.; Miao, X.; Zeng, J.; Li, X.; Dong, Y.; Li, Y.; Bian, F.; You, J. Structure evolution of PVDF/PBSU interpenetrating crystal frameworks during deformation investigated by in-situ synchrotron radiation SAXS/WAXS. *Giant* **2025**, *22*, 100354.
21 Muller, A. J.; Balsamo, V.; Arnal, M. L.; Jakob, T.; Schmalz, H.; Abetz, V. Homogeneous nucleation and fractionated crystallization in block copolymers. *Macromolecules* **2002**, *35*, 3048−3058.
22 Lorenzo, A. T.; Arnal, M. L.; Sanchez, J. J.; Muller, A. J. Effect of annealing time on the self-nucleation behavior of semicrystalline polymers. *J. Polym. Sci. B: Polym. Phys.* **2006**, *44*, 1738−1750.
23 Trujillo, M.; Arnal, M. L.; Müller, A. J.; Laredo, E.; Bredeau, S.; Bonduel, D.; Dubois, P. Thermal and morphological characterization of nanocomposites prepared by in-situ polymerization of high-density polyethylene on carbon nanotubes. *Macromolecules* **2007**, *40*, 6268−6276.
24 Lorenzo, A. T.; Arnal, M. L.; Müller, A. J.; Lin, M.-C.; Chen, H.-L. SAXS/DSC analysis of the lamellar thickness distribution on a SSA thermally fractionated model polyethylene. *Macromol. Chem. Phys.* **2011**, *212*, 2009−2016.
25 Sangroniz, L.; Cavallo, D.; Muller, A. J. Self-nucleation effects on polymer crystallization. *Macromolecules* **2020**, *53*, 4581−4604.
26 Liu, X.; Yu, W. Role of chain dynamics in the melt memory effect of crystallization. *Macromolecules* **2020**, *53*, 7887−7898.
27 Arandia, I.; Mugica, A.; Zubitur, M.; Arbe, A.; Liu, G.; Wang, D.; Mincheva, R.; Dubois, P.; Müller, A. J. How composition determines the properties of isodimorphic poly(butylene succinate-ran-butylene azelate) random biobased copolymers: from single to double crystalline random copolymers. *Macromolecules* **2015**, *48*, 43−57.
28 Liu, X. R.; Wang, Y.; Wang, Z. F.; Cavallo, D.; Muller, A. J.; Zhu, P.; Zhao, Y.; Dong, X.; Wang, D. J. The origin of memory effects in the crystallization of polyamides: role of hydrogen bonding. *Polymer* **2020**, *188*, 122117.
29 Fernández-Tena, A.; Pérez-Camargo, R. A.; Coulembier, O.; Sangroniz, L.; Aranburu, N.; Guerrica-Echevarria, G.; Liu, G.; Wang, D.; Cavallo, D.; Müller, A. J. Effect of molecular weight on the crystallization and melt memory of poly(ε-caprolactone) (PCL). *Macromolecules* **2023**, *56*, 4602−4620.
30 Sangroniz, L.; Müller, A. J.; Cavallo, D. Origin of melt memory effects in poly(ethylene oxide): the crucial role of entanglements. *Macromol. Rap. Comm.* **2024**, *45*, 2400011.
31 AliAboudzadeh, M.; Sangroniz, L.; Coulembier, O.; Ferranti, M.; Costanzo, S.; Grizzuti, N.; Cavallo, D.; Müller, A. J. Decoupling the roles of chain length, entanglements and intermolecular interactions on the melt memory of semicrystalline homopolymers. *Macromolecules* **2026**, *59*, 3371−3383.
32 Rubinstein, M.; Colby, R. H. *Polymer Physics*; Oxford University Press, **2003**, p. 361−422.
33 Wang, Z.; Zeng, J.; Liang, Y.; Zhang, R.; Zhu, C.; Xu, J.; Müller, A. J. The effect of entanglement concentration on the melt memory of polyethylene random copolymer. *Polymer* **2025**, *332*, 128576.
34 Gao, H.; Vadlamudi, M.; Alamo, R. G.; Hu, W. Monte carlo simulations of strong memory effect of crystallization in random copolymers. *Macromolecules* **2013**, *46*, 6498−6506.
35 Reid, B. O.; Vadlamudi, M.; Mamun, A.; Janani, H.; Gao, H.; Hu, W.; Alamo, R. G. Strong memory effect of crystallization above the equilibrium melting point of random copolymers. *Macromolecules* **2013**, *46*, 6485−6497.
36 Chen, X.; Mamun, A.; Alamo, R. G. Effect of level of crystallinity on melt memory bove the equilibrium melting temperature in a random ethylene 1-utene copolymer. *Macromol. Chem. Phys.* **2015**, *216*, 1220−1226.
37 Chen, X.; Wignall, G. D.; He, L.; Lopez-Barron, C.; Alamo, R. G. SANS Evidence of liquid–liquid phase separation leading to inversion of crystallization rate of broadly distributed random ethylene copolymers. *Macromolecules* **2017**, *50*, 4406−4414.
38 Michell, R. M.; Mugica, A.; Zubitur, M.; Muller, A. J. Self-Nucleation of crystalline phases within homopolymers, polymer blends, copolymers, and nanocomposites. In *Polymer Crystallization I: From Chain Microstructure to Processing*, Auriemma, F., Alfonso, G. C., DeRosa, C. Eds.; Advances in Polymer Science, Vol. 276; Springer, **2017**, p. 215.
39 Sangroniz, L.; Cavallo, D.; Santamaria, A.; Müller, A. J.; Alamo, R. G. Thermorheologically complex self-seeded melts of propylene–ethylene copolymers. *Macromolecules* **2017**, *50*, 642−651.
40 Chen, X.; López-Barrón, C.; Zeng, Y.; Alamo, R. G. Concentration fluctuations in the early stages of LLPS and partial dissolution of melt-memory in broadly distributed ethylene copolymers. *Polymer* **2018**, *148*, 181−190.
41 Liu, P.; Xue, Y.; Men, Y. Melt Memory Effect beyond the equilibrium melting point in commercial isotactic polybutene-1. *Ind. Eng. Chem. Res.* **2019**, *58*, 5472−5478.
42 Ren, M.; Chen, X.; Sang, Y.; Alamo, R. G. Comparative effects on recrystallization of melt-memory and liquid–liquid phase separation in Ziegler–Natta and metallocene ethylene copolymers with bimodal comonomer composition distribution. *Ind. Eng. Chem. Res.* **2020**, *59*, 19260−19271.
43 Liao, Y.; Pan, L.; Ma, Z.; Cavallo, D.; Liu, G.; Wang, D.; Müller, A. J. How 4-(7-Octen-1-yl)-N,N-diphenylaniline co-units induce strong melt memory effects in isotactic polypropylene random

copolymers. *Polymer* **2023**, *282*, 126184.
44 Ruland, W. The evaluation of the small-angle scattering of lamellar two-phase systems by means of interface distribution functions. *Colloid Polym. Sci.* **1977**, *255*, 417–427.
45 Seidlitz, A.; Thurn-Albrecht, T. Small-angle X-ray scattering for morphological analysis of semicrystalline polymers. In *Polymer morphology*, John Wiley & Sons, Inc, **2016**, pp. 151–164.
46 Schulz, M.; Seidlitz, A.; Kurz, R.; Bärenwald, R.; Petzold, A.; Saalwächter, K.; Thurn-Albrecht, T. The Underestimated Effect of Intra-crystalline chain dynamics on the morphology and stability of semicrystalline polymers. *Macromolecules* **2018**, *51*, 8377–8385.
47 Schäfer, M.; Wallstein, N.; Schulz, M.; Thurn-Albrecht, T.; Saalwächter, K. Intra-crystalline dynamics in oligomer-diluted poly(ethylene oxide). *Macromol. Chem. Phys.* **2020**, *221*, 1900393.
48 Schulz, M.; Schäfer, M.; Saalwächter, K.; Thurn-Albrecht, T. Competition between crystal growth and intracrystalline chain diffusion determines the lamellar thickness in semicrystalline polymers. *Nat. Comm.* **2022**, *13*, 119.
49 Yu, Q.; Anuar, A.; Petzold, A.; Balko, J.; Saalwächter, K.; Thurn-Albrecht, T. The semicrystalline morphology of polybutylene succinate supports a general scheme based on intracrystalline dynamics. *Macromol. Chem. Phys.* **2023**, *224*, 2200459.
50 Ferry, J. D. *Viscoelastic Properties of Polymers*; Wiley, 1970.
51 van Ruymbeke, E.; Masubuchi, Y.; Watanabe, H. Effective value of the dynamic dilution exponent in bidisperse linear polymers: from 1 to 4/3. *Macromolecules* **2012**, *45*, 2085–2098.
52 Shahid, T.; Huang, Q.; Oosterlinck, F.; Clasen, C.; van Ruymbeke, E. Dynamic dilution exponent in monodisperse entangled polymer solutions. *Soft Matter* **2017**, *13*, 269–282.
53 Lauritzen, J.; Hoffman, J. Extension of theory of growth of chain-folding polymer crystals to large undercoolings. *J. Appl. Phys.* **1973**, *44*, 4340–4352.
54 Hoffman, J. D.; G, T. D.; Lauritzen, J. I. The rate of crystallization of linear polymers with chain folding. In *Treatise on Solid State Chemistry*, Hannay, N. B. Ed.; Springer-Verlag US, **1976**, p. 497.
55 Wunderlich, B. in *Macromolecular Physics*, Academic Press, **1976**, p. 1–114.
56 Wunderlich, B. Molecular nucleation and segregation. *Faraday Discuss. Chem. Soc.* **1979**, *68*, 239–243.
57 Zhang, R.; Du, M.; Jariyavidyanont, K.; Androsch, R.; Zhuravlev, E.; Schick, C. Fast scanning calorimetry of semicrystalline polymers: from fundamental research to industrial applications. *Acc. Chem. Res* **2025**, *6*, 627–637.
58 Huang, Y. L.; Brown, N. The effect of molecular weight on slow crack growth in linear polyethylene homopolymers. *J. Mater. Sci.* **1988**, *23*, 3648–3655.
59 Qiao, Y. N.; Men, Y. F. Intercrystalline links determined kinetics of Form II to I polymorphic transition in polybutene-1. *Macromolecules* **2017**, *50*, 5490–5497.
60 Huang, Y.; Xu, Z. D.; Huang, Y. P.; Ma, D. Z.; Yang, J. C.; Mays, J. W. Characterization of poly(epsilon-caprolactone) *via* size exclusion chromatography with online right-angle laser-light scattering and viscometric detectors. *Int. J. Polym. Anal. Charact.* **2003**, *8*, 383–394.
61 Schulz, M.; Seidlitz, A.; Petzold, A.; Thurn-Albrecht, T. The effect of intra-crystalline chain dynamics on melting and reorganization during heating in semicrystalline polymers. *Polymer* **2020**, *196*, 122441.
62 Blundell, D. J.; Keller, A.; Kovacs, A. J. A new self-nucleation phenomenon and its application to the growing of polymer crystals from solution. *J. Polym. Sci. B: Polym. Phys.* **1966**, *4*, 481–486.
63 Blundell, D. J.; Keller, A. Nature of self-seeding polyethylene crystal nuclei. *J. Macromol. Sci. B Phys*. **1968**, *2* 301–336.
64 Fillon, B.; Thierry, A.; Wittmann, J. C.; Lotz, B. Self-nucleation and recrystallization of polymers - isotactic polypropylene, beta-phase - beta-alpha-conversion and beta-alpha-growth transitions. *J. Polym. Sci. B: Polym. Phys.* **1993**, *31*, 1407–1424.
65 Pérez, R. A.; Córdova, M. E.; López, J. V.; Hoskins, J. N.; Zhang, B.; Grayson, S. M.; Müller, A. J. Nucleation, crystallization, self-nucleation and thermal fractionation of cyclic and linear poly(ε-caprolactone)s. *React. Funct. Polym.* **2014**, *80*, 71–82.
66 Sangroniz, L.; Sangroniz, A.; Meabe, L.; Basterretxea, A.; Sardon, H.; Cavallo, D.; Müller, A. J. Chemical structure drives memory effects in the crystallization of homopolymers. *Macromolecules* **2020**, *53*, 4874–4881.
67 Sangroniz, L.; Jang, Y.-J.; Hillmyer, M. A.; Müller, A. J. The role of intermolecular interactions on melt memory and thermal fractionation of semicrystalline polymers. *J. Chem. Phys*. **2022**, *156*, 144902.
68 Sangroniz, L.; Safari, M.; Martínez de Ilarduya, A.; Sardon, H.; Cavallo, D.; Müller, A. J. Disappearance of melt memory effect with comonomer incorporation in isodimorphic random copolyesters. *Macromolecules* **2023**, *56*, 7879–7888.
69 Androsch, R.; Di Lorenzo, M. L. Crystal nucleation in glassy poly(l-lactic acid). *Macromolecules* **2013**, *46*, 6048–6056.
70 Lemstra, P. J. Chapter 1: High-performance polyethylene fibers. *Adv. Ind. Eng. Polym. Res.* **2022**, *5*, 49–59.
71 Wang, Z.; Li, B.; Christakopoulos, F.; Xie, K.; Zhu, C.; Xu, J.; Müller, A. J. Structure formation and unexpected ultrafast re-entanglement dynamics of disentangled ultrahigh molecular weight polyethylene. *Macromolecules* **2024**, *57*, 10240–10252
72 Wang, Z.; Sangroniz, L.; Xu, J.; Zhu, C.; Müller, A. Polymer Physics behind the Gel-Spinning of UHMWPE Fibers. *Macromol. Rapid Commun.* **2024**, *45*, 2400124.

https://doi.org/10.1007/s10118-026-3695-5